



**HAL**  
open science

## Formation of nanocrystalline diamond at Low Temperature by MicroWave plasma microtorch

Zixian Jia, Youcef Fermi, Ovidiu Brinza, Khaled Hassouni, Swaminathan Prasanna

► **To cite this version:**

Zixian Jia, Youcef Fermi, Ovidiu Brinza, Khaled Hassouni, Swaminathan Prasanna. Formation of nanocrystalline diamond at Low Temperature by MicroWave plasma microtorch. 2021. hal-03205281

**HAL Id: hal-03205281**

**<https://hal.science/hal-03205281v1>**

Preprint submitted on 22 Apr 2021

**HAL** is a multi-disciplinary open access archive for the deposit and dissemination of scientific research documents, whether they are published or not. The documents may come from teaching and research institutions in France or abroad, or from public or private research centers.

L'archive ouverte pluridisciplinaire **HAL**, est destinée au dépôt et à la diffusion de documents scientifiques de niveau recherche, publiés ou non, émanant des établissements d'enseignement et de recherche français ou étrangers, des laboratoires publics ou privés.

# Formation of nanocrystalline diamond at Low Temperature by MicroWave plasma microtorch

Zixian JIA, Youcef FERMI, Ovidiu BRINZA, Khaled HASSOUNI, Swaminathan PRASANNA\*

## Abstract

Producing high quality nanodiamonds at near ambient conditions remains challenging. In this work, we report the synthesis of nanodiamond at low temperature using microwave plasma microtorch by dissociation of CH<sub>4</sub>/H<sub>2</sub>. The TEM, Raman and EELS spectra confirm the presence of sp<sup>3</sup> carbon. The TEM and SEM image indicated that the grain of diamond is about 10 nm. In addition, the influence of power for diamond growth was also investigated. The sp<sup>3</sup>/sp<sup>2</sup> increase with increasing power while the I<sub>D</sub>/I<sub>G</sub> ratio decreases.

## 1. Introduction

The unique properties of nanodiamonds including high hardness, high thermal conductivity, chemical stability and biocompatibility find application in a wide range of areas such as drug delivery, biomarkers, tribological applications and quantum technologies [1]. Today, many techniques were investigated to achieve nanodiamond by detonation [2], laser ablation [3], high-pressure high-temperature technique (HPHT) [4], ion irradiation of graphite [5] and Plasma-enhanced chemical vapor deposition (PECVD) [6]. The last has been considered as better solution compared to other process due to simple operation and low injected power. By the PECVD technique, diamond is synthesized by activating an H<sub>2</sub> / CH<sub>4</sub> gas mixture rich in hydrogen under low-pressure conditions where the graphite phase is thermodynamically the most stable. The production of atomic hydrogen then plays an essential role in stabilization of the diamond phase by saturating the pendant bonds at the surface and by ensuring the etching of the non-diamond phases that could co-deposit (sp<sup>2</sup> carbon). Methyl radicals (CH<sub>3</sub>) also produced from the dissociation of methane are considered to be the main precursor carbon species [7].

Using PECVD for diamond deposition generally require a high substrate temperature (>700°C) [8]. With the reactor MW (MicroWave)-PECVD developed in our team [9][10], it is possible to grow low-dislocation diamond [11] and high NV density diamond [12]. However, because of the requirements in many applications in electronics, medicine and

biology, the synthesis of diamond (films or nanoparticles) at temperatures  $< 500^{\circ}\text{C}$ , especially at room temperature, is highly requested. Using optimized ultrasonic seeding process, Xiao *et al.*[13] obtained dense and continuous ultrananocrystalline diamond at temperatures as low as  $400^{\circ}\text{C}$ . Even, the diamond films was obtained by the halogenated [14] and oxygen [6][15] containing precursors at low temperature. In our study, we present a new route to synthesize the nanodiamond at room temperature using a home-made microwave plasma microtorch based on coaxial transmission line resonators providing high electron densities, charged species, radicals and photons. The dissociation of gas mixture was followed by optical emission spectroscopy (OES). The structure of carbon nanoparticles was analyzed by micro Raman and TEM. Additional microstructural characterization of our material was performed by SEM and TEM. The influence of the injected power on diamond growth was also studied.

## **2. Experiments and methods**

### **2.1 Microwave plasma reactor**

The experimental set-up for the synthesis of nanodiamonds by microwave (MW) Plasma Enhanced Chemical Vapor Deposition (PECVD) is schematically illustrated in Fig. 1. The MW plasma microtorch (Fig. S1) was developed in-house based on coaxial transmission line resonators (CLTR) [16]. The present torch can be operated for different gas mixtures such as Ar/H<sub>2</sub>/methane/acetylene/ethanol and a wide range of pressure conditions (10 mbar – 1 atm). It provides a distinct advantage of producing highly non-equilibrium discharges which can realize a wide range of reactive environments with high electron densities, charged species, radicals and photons over dimensions limited to a few millimetres. A variety of local plasma conditions can be obtained in this very flexible plasma torch which makes it possible to explore a wide range of non-equilibrium nucleation routes of carbon NPs, especially DNPs.

With the doubled-walled and water-cooled plasma torch, a copper tube located within the reactor was used to pass a mixture of gas stream (CH<sub>4</sub> + H<sub>2</sub>) through a microwave guide. This stream was used to generate hydrogen plasma. Methane inside the plasma had a residence time on the order of  $10^{-1}$  s and rapidly dissociated in the plasma, forming carbon matter. After passing through the plasma, reaction products were collected downstream on Si substrate or a fiber glass filter. Certified gas cylinders are supplied by Air Liquid. The pressure of reactor chamber was kept at 100 mbar by a Bronkhorst pressure regulator. The optical emission of MW plasma was collected with a 600 micrometer diameter fiber optic cable coupled to a

spectrograph with a focal length of 1 m (THR1000). Spectra were integrated 10 times with an acquisition time of 100 ms.

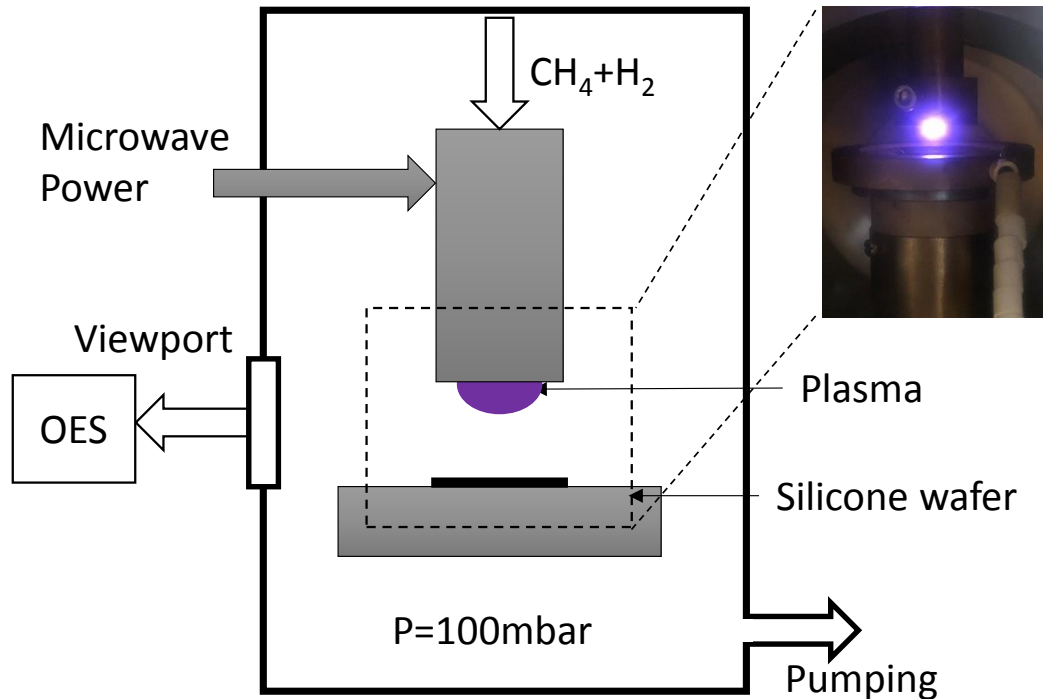


*Figure 1. MPCVD reactor and OES set up*

## 2.2 Characterization

The Raman spectra of the samples at room temperature were measured in the backscattering configuration using a HR800 spectrometer equipped with a Peltier-cooled CCD detector (Horiba Jobin Yvon) with spectral and spatial resolutions of  $0.25 \text{ cm}^{-1}$  and  $5 \mu\text{m}$ , respectively. Raman measurements were carried out by focusing the probe beam at  $473 \text{ nm}$  with a  $50\times$  objective on the carbon particles.

Scanning electron microscopy (SEM) (Zeiss Supra 40 VP SEM-FEG) was used to observe the morphology of carbon nanoparticles. TEM observation was performed in a JEOL 200 kV microscope with the carbon nanoparticles suspension drop-casted onto a carbon TEM grid.

## 3. Results and Discussion

### 3.1 Nanocrystalline diamond formation

Fig. 2a shows the SEM microstructure of carbon nanoparticles deposited by MW-PECVD on Si substrate. The particles with a grain size around  $10 \text{ nm}$  and EDX shows that the particles

contain only C, O and Si (The present of O and Si is due to the substrate). The original and fitted Raman spectra have been presented in Fig. 2c for a laser excitation at 473 nm. The 1129  $\text{cm}^{-1}$  peak is assigned to the  $\nu_1$  mode of transpolyacetylene [17]. The  $\text{C}_2$  radical serve precursors for nanocrystalline diamond and also likely for unsaturated carbon chains such as  $(-\text{C}^*=\text{C}^*_-)$  through addition polymerization. The hydrogen atoms in a hydrogen-rich plasmas terminate the dangling bonds (\*) for stabilization and form transpolyacetylene. For bulk diamond with the high crystalline quality, a sharp peak at 1332  $\text{cm}^{-1}$  is commonly used as a signature. Nevertheless, in our case (room temperature and low pressure), the formation of diamond was not under optimum conditions which provides small grain size. Consequently, due to the phonon confinement, the asymmetrical broadening was observed and this diamond peak was blue shifted to 1329  $\text{cm}^{-1}$  for nm-scale diamond [18]. The 1385 and 1598  $\text{cm}^{-1}$  peaks correspond to the  $\text{sp}^2$  carbon D peak and the  $\text{sp}^2$  carbon G peak respectively [19].

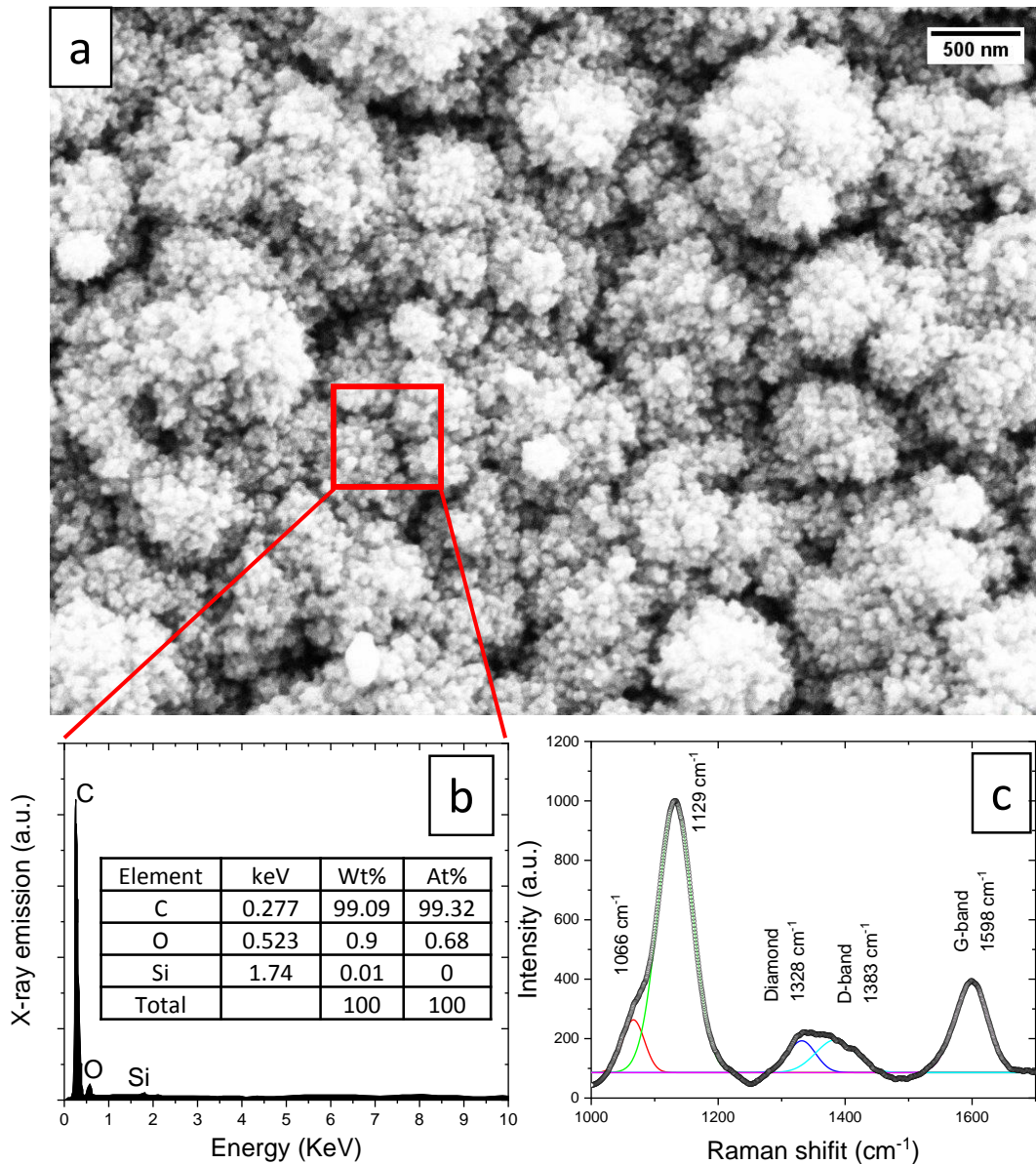
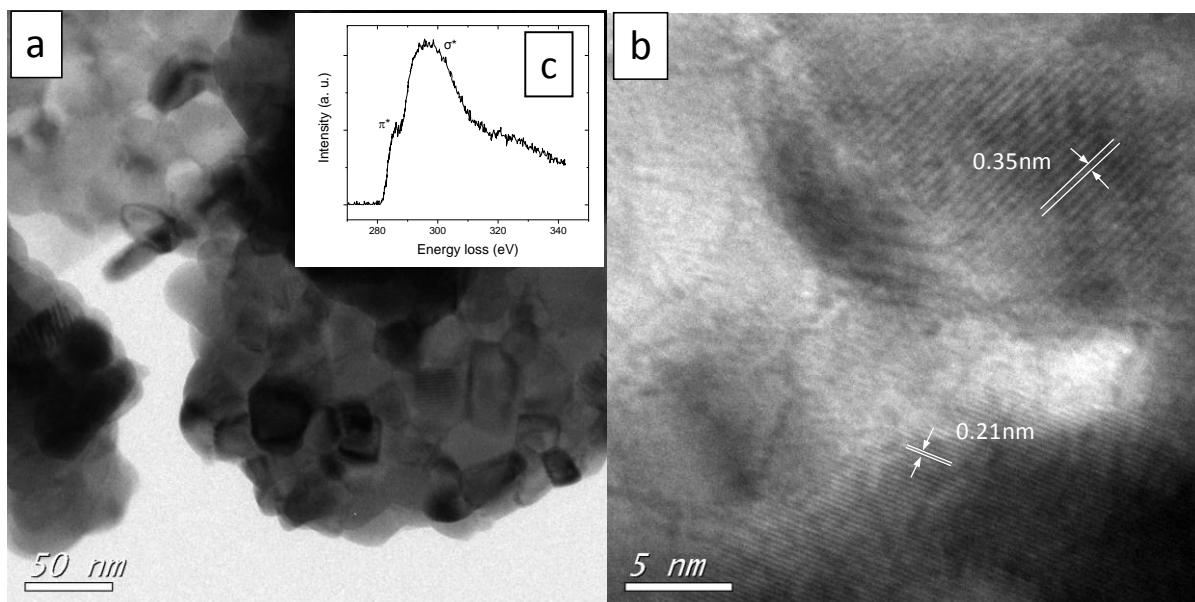


Figure 2. Material characterization of carbon nanoparticles deposited on Si substrate. a) SEM image carbon nanoparticles, b) its corresponding EDX spectra, and c) Micro Raman spectra. (Experimental conditions:  $CH_4 = 4$  sccm,  $H_2 = 96$  sccm, Distance between plasma torch and substrate = 5mm, Frequency of microwave = 2480 Hz, Pressure of reactor = 100 mbar, Injected power = 90 W, Deposition time = 60 min and Temperature = Room temperature.)

Furthermore, the size of nanodiamond was confirmed by TEM images shown in Fig. 3. Similar to the SEM image in Fig. 2a, Fig. 3a shows the agglomerated microstructure of the carbon nanoparticles with a diameter of around 10 nm. Under the plasma synthesis, the hybrid nanostructure in which both graphitic carbon and diamond crystal were observed as shown in

Fig 3b. The d-spacings of 0.21 nm and 0.35 nm are in consistent with diamond (111) plane and graphite (002) plane, respectively. EELS spectra in Fig. 4c showed the  $1s \rightarrow \sigma^*$  which corresponds to  $sp^3$ -hybridised carbon. The presence of some amount of  $sp^2$  carbon is also indicated by  $1s \rightarrow \pi^*$  feature.



*Figure 3. TEM image of carbon nanoparticles of different resolution a) 50nm and b) 5nm; c) its corresponding EEL spectra. (Experimental conditions:  $CH_4 = 4$  sccm,  $H_2 = 96$  sccm, Distance between plasma torch and substrate = 5mm, Frequency of microwave = 2480 Hz, Pressure of reactor = 100 mbar, Injected power = 90 W, Deposition time = 60 min and Temperature = Room temperature.)*

### 3.3 The influence of power

The gas temperature that plays a key role in gas phase chemistry depends on the injected power. In our experiment, the dissociation of  $CH_4$  and  $H_2$  was recorded in-situ by optical emission spectroscopy (OES). Here, the  $H_2$  Fulcher- $\alpha$  band was used to estimate the experimental  $H_2$  rotational temperatures. An example of the measured  $H_2$  Fulcher- $\alpha$  band Q-branch spectrum is shown in Fig. S1a, where the Boltzmann plot corresponding to  $Q_1$ ,  $Q_2$ ,  $Q_3$  and  $Q_6$  selected rotational lines is shown in the Fig. S1b. As shown in Fig. 4(a), increasing the injected power from 30 to 90 W increases the  $H_2$  rotational temperatures from 525 to 760 K. By increasing the injected power, more energy was transferred from electric field to the gas

molecules by electrons during collisions that induce the rise in gas temperature. Moreover, the  $H_2$  rotational temperatures is relatively lower than others reported data [20][21].

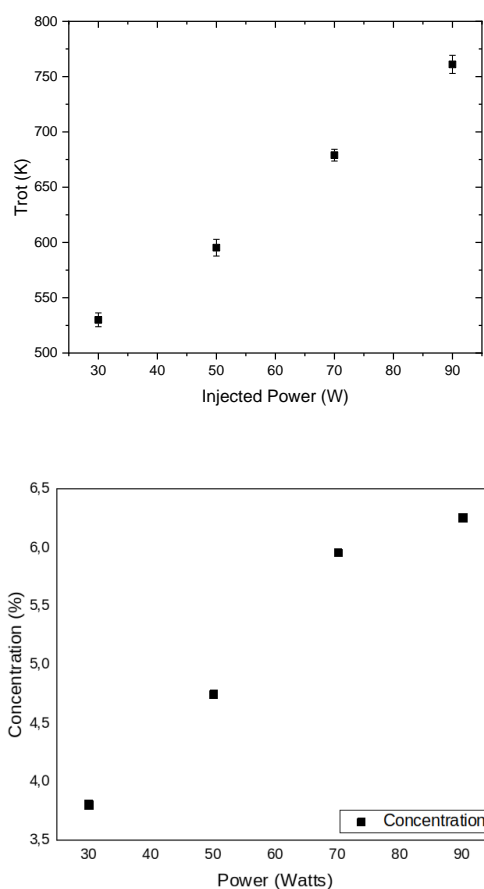
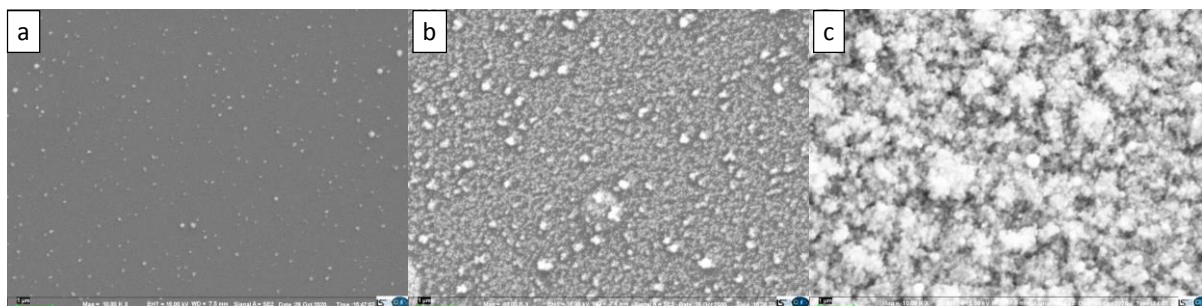


Figure 4. (a)  $H_2$  rotational temperature measured by OES (b) concentration of H-atoms measured by actinometry [22] as a function of input microwave power.

The influence of input power on diamond growth is presented in Fig. 5 for three different power: 30, 70 and 90W. In our plasma reactor, no heating has been applied to the substrate surface and the Si substrate temperature was almost stable ( $\sim 343.15K$ ) during the experiments in a range of input powers 30 to 90W. Moreover, the signature of Raman spectra of the NPs collected were very similar when the distance of the substrate from the plasma source was changed or when the duration of the experiments were changed between 5 minutes and 60 minutes. Therefore, it can be considered that the diamond particle formation may mainly occur in the gas phase and the substrate served as sample collector. Similar substrate-free microwave plasma reactors have been used in the past to synthesize various materials [6][23]. Consequently, the change of morphology observed in Fig.5 should be related to the gas phase chemistry. The  $H_2$  rotational temperatures increase with the input power. As a consequence,

the concentration of atomic H also increases. Moreover, the high input power should provide a highly reactive plasma conditions which enables degradation of CH<sub>4</sub> to produce enough chemical C1 species(CH<sub>3</sub>, CH<sub>2</sub> and CH). The C1 species along with high concentrations of hydrogen should be conducive towards the growth of nanodiamond [24][25].



*Figure 5. The effect of power on diamond formation. SEM images of carbon nanoparticles deposited on Si substrate applied different injected power: a) 30W, b) 70W and c) 90W. (Experimental conditions: CH<sub>4</sub> = 4 sccm, H<sub>2</sub> = 96 sccm, Distance between plasma torch and substrate = 5mm, Frequency of microwave =2480 Hz, Pressure of reactor = 100 mbar, Deposition time = 60 min and Temperature = Room temperature.)*

In order to better understand the influence of power on diamond growth, the Raman spectra of the samples obtained with different input power is analyzed (Fig. S3) and the sp<sup>3</sup>/sp<sup>2</sup> and I<sub>D</sub>/I<sub>G</sub> ratio is presented in Fig. 6. The power has a positive effect on sp<sup>3</sup> carbon formation as more hydrogen atoms were dissociated with higher injected power. These H atoms play important roles for H-shifting reaction of CH<sub>4</sub> producing CH<sub>x</sub> radicals. The ratio between [H] and [CH<sub>x</sub>] is crucial for the diamond nucleation and growth [25]. That is why no sp<sup>3</sup> carbon was detected with a power below 70W. In addition, the I<sub>D</sub>/I<sub>G</sub> ratio decreases from 0.53 to 0.33 with increasing power. Similar results have been reported in the literature that I<sub>D</sub>/I<sub>G</sub> ratio, which decreases with increasing sp<sub>3</sub> fraction in the amorphous carbon films [26,27].

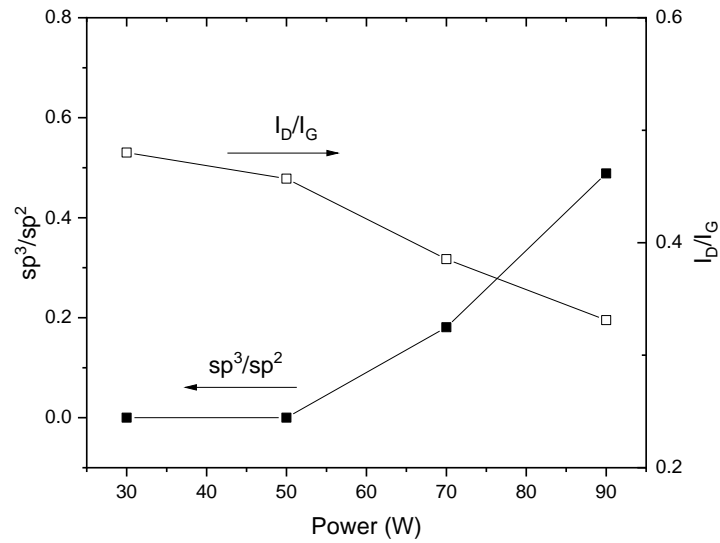


Figure 6. the  $sp^3/sp^2$  (left) and  $I_D/I_G$  (right) ratio as a function of input power ( $sp^3/sp^2$  bonds ratio is calculated from the intensity of the diamond peak at  $1328\text{ cm}^{-1}$  and the intensity of the G band about  $1583\text{ cm}^{-1}$ );

Even if the mechanism of diamond formation is not the focus of this study, we still try to give the possible reasons to explain the nanodiamond formation in our process involving the gas phase chemistry. Previous studies by homogenous nucleation have produced diamond nanoparticles using  $\text{CH}_4\text{-CO}_2$  [28] or ethanol [6]. H atoms and  $\text{CH}_3$  radicals are generally considered as key constituents in most diamond CVD environments. H atoms could preferentially etch non-diamond carbon and enable the growth of diamond-phase carbon [29]. This reaction should contribute to the nanodiamond formation in our process as both diamond-phase carbon and graphite were observed by TEM. Apart from the etching, sufficient H atom could help initiate the processes responsible for diamond grows by preventing the C1 species to produce non-diamond carbon. Future research is needed to better understand the mechanism for nanodiamond formation in our method, as well as to distinguish between kinetic and thermodynamic aspects.

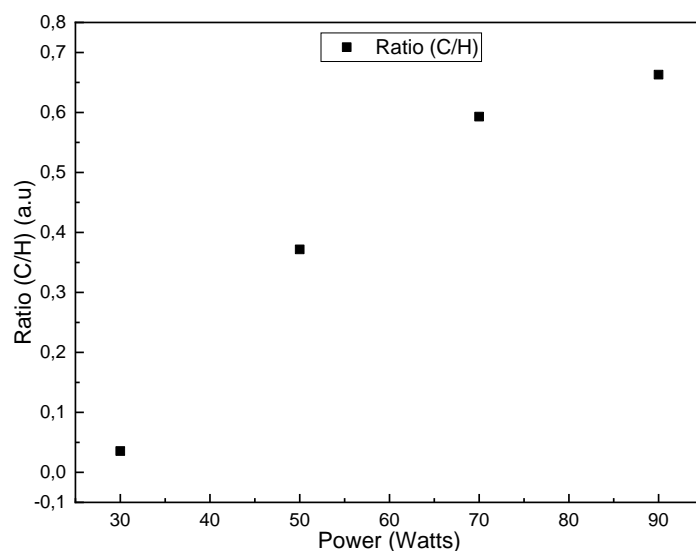


Figure 7. The relative abundance of  $C_2$  radical to H-atom concentration evaluated from the ratio of intensities of  $I(C_2 \text{ Swann})$  and H-alpha as a function of input power

Further, we find a positive correlation between the relative concentrations of  $C_2$  radical (measured from the ratio of intensities of  $C_2$  Swann to H-alpha) as seen in Figure 7 and the amount of  $sp^3$  DNPs as estimated from Raman. This shows the need to investigate whether  $C_2$  is a key precursor of DNPs nucleation or just an indicative species of enhanced DNPs nucleation.

#### 4. Conclusion

We have developed a process for nanodiamond synthesis using microwave plasma enhanced chemical vapor deposition by dissociation of  $CH_4/H_2$ . The reactor could be work at room temperature, substrate-free condition and avoid the impurities (nitrogen and oxygen). The band of  $1329 \text{ cm}^{-1}$  observed in RAMAN spectra and the EELS spectra confirm the diamond formation. The TEM and SEM image indicated that the grain of diamond is about 10 nm. The effect of power on diamond growth was investigated. OES spectra shows that the  $H_2$  rotational temperature increases with the increasing power which may be the reason of the increasing  $sp^3/sp^2$  ratio. The influence of  $CH_4/H_2$  ratio, pressure of the reaction and addition of argon will be investigated.

## Acknowledgments

"ANR (Agence Nationale de la Recherche) and CGI (Commissariat à l'Investissement d'Avenir) are gratefully acknowledged for their financial support of this work through Labex SEAM (Science and Engineering for Advanced Materials and devices), ANR-10-LABX-0096 and ANR-18-IDEX-0001".

One of the author (Khaled Hassouni) acknowledge the support of the Institut Universitaire de France.

## Reference

- [1] V.N. Mochalin, O. Shenderova, D. Ho, Y. Gogotsi, The properties and applications of nanodiamonds, *Nat. Nanotechnol.* 7 (2012) 11–23. doi:10.1038/nnano.2011.209.
- [2] A. Krüger, F. Kataoka, M. Ozawa, T. Fujino, Y. Suzuki, A.E. Aleksenskii, A.Y. Vul', E. Osawa, Unusually tight aggregation in detonation nanodiamond: Identification and disintegration, *Carbon N. Y.* 43 (2005) 1722–1730. doi:10.1016/j.carbon.2005.02.020.
- [3] D. Amans, A.C. Chénus, G. Ledoux, C. Dujardin, C. Reynaud, O. Sublemontier, K. Masenelli-Varlot, O. Guillois, Nanodiamond synthesis by pulsed laser ablation in liquids, *Diam. Relat. Mater.* 18 (2009) 177–180. doi:10.1016/j.diamond.2008.10.035.
- [4] J. Qian, C. Pantea, J. Huang, T.W. Zerda, Y. Zhao, Graphitization of diamond powders of different sizes at high pressure-high temperature, *Carbon N. Y.* 42 (2004) 2691–2697. doi:10.1016/j.carbon.2004.06.017.
- [5] T.L. Daulton, M.A. Kirk, R.S. Lewis, L.E. Rehn, Production of nanodiamonds by high-energy ion irradiation of graphite at room temperature, in: *Nucl. Instruments Methods Phys. Res. Sect. B Beam Interact. with Mater. Atoms*, North-Holland, 2001: pp. 12–20. doi:10.1016/S0168-583X(00)00603-0.
- [6] A. Kumar, P. Ann Lin, A. Xue, B. Hao, Y. Khin Yap, R.M. Sankaran, Formation of nanodiamonds at near-ambient conditions via microplasma dissociation of ethanol vapour, *Nat. Commun.* 4 (2013) 1–9. doi:10.1038/ncomms3618.
- [7] J.E. Butler, Y.A. Mankelevich, A. Cheesman, J. Ma, M.N.R. Ashfold, Understanding the chemical vapor deposition of diamond: Recent progress, *J. Phys. Condens. Matter.* (2009). doi:10.1088/0953-8984/21/36/364201.
- [8] A. Gicquel, K. Hassouni, F. Silva, J. Achard, CVD diamond films: From growth to applications, *Curr. Appl. Phys.* 1 (2001) 479–496. doi:10.1016/S1567-1739(01)00061-X.
- [9] K. Hassouni, F. Silva, A. Gicquel, Modelling of diamond deposition microwave cavity

- generated plasmas, *J. Phys. D. Appl. Phys.* (2010). doi:10.1088/0022-3727/43/15/153001.
- [10] A. Gicquel, F. Silva, C. Rond, N. Derkaoui, O. Brinza, J. Achard, G. Lombardi, A. Tallaire, A. Michau, M. Wartel, K. Hassouni, Ultrafast Deposition of Diamond by Plasma-Enhanced CVD, in: *Compr. Hard Mater.*, 2014. doi:10.1016/B978-0-08-096527-7.00047-7.
- [11] A. Tallaire, O. Brinza, V. Mille, L. William, J. Achard, Reduction of Dislocations in Single Crystal Diamond by Lateral Growth over a Macroscopic Hole, *Adv. Mater.* (2017). doi:10.1002/adma.201604823.
- [12] A. Tallaire, O. Brinza, P. Huillery, T. Delord, C. Pellet-Mary, R. Staacke, B. Abel, S. Pezzagna, J. Meijer, N. Touati, L. Binet, A. Ferrier, P. Goldner, G. Hetet, J. Achard, High NV density in a pink CVD diamond grown with N<sub>2</sub>O addition, *Carbon N. Y.* (2020). doi:10.1016/j.carbon.2020.08.048.
- [13] X. Xiao, J. Birrell, J.E. Gerbi, O. Auciello, J.A. Carlisle, Low temperature growth of ultrananocrystalline diamond, *J. Appl. Phys.* 96 (2004) 2232–2239. doi:10.1063/1.1769609.
- [14] I. Schmidt, C. Benndorf, Low temperature CVD diamond deposition using halogenated precursors - Deposition on low melting materials: Al, Zn and glass, *Diam. Relat. Mater.* 10 (2001) 347–351. doi:10.1016/S0925-9635(00)00434-9.
- [15] D. Dekkar, A. Puth, E. Bisceglia, P.W.P. Moreira, A. V. Pipa, G. Lombardi, J. Röpecke, J.H. Van Helden, F. Bénédic, Effect of the admixture of N<sub>2</sub> to low pressure, low temperature H<sub>2</sub>-CH<sub>4</sub>-CO<sub>2</sub> microwave plasmas used for large area deposition of nanocrystalline diamond films, *J. Phys. D. Appl. Phys.* 53 (2020) 455204. doi:10.1088/1361-6463/aba7df.
- [16] J. Choi, F. Iza, H.J. Do, J.K. Lee, M.H. Cho, Microwave-excited atmospheric-pressure microplasmas based on a coaxial transmission line resonator, *Plasma Sources Sci. Technol.* 18 (2009) 25029. doi:10.1088/0963-0252/18/2/025029.
- [17] A.C. Ferrari, J. Robertson, Origin of the 1150 – cm<sup>-1</sup> Raman mode in nanocrystalline diamond, *Phys. Rev. B - Condens. Matter Mater. Phys.* 63 (2001) 121405. doi:10.1103/PhysRevB.63.121405.
- [18] V.I. Korepanov, H. o. Hamaguchi, E. Osawa, V. Ermolenkov, I.K. Lednev, B.J.M. Etzold, O. Levinson, B. Zousman, C.P. Epperla, H.C. Chang, Carbon structure in nanodiamonds elucidated from Raman spectroscopy, *Carbon N. Y.* 121 (2017) 322–329. doi:10.1016/j.carbon.2017.06.012.
- [19] A.C. Ferrari, J. Robertson, Raman spectroscopy of amorphous, nanostructured, diamond-like carbon, and nanodiamond, *Philos. Trans. R. Soc. A Math. Phys. Eng. Sci.* 362 (2004) 2477–2512. doi:10.1098/rsta.2004.1452.

- [20] D. Dekkar, A. Puth, E. Bisceglia, P.W.P. Moreira, A. V. Pipa, G. Lombardi, J. Röpcke, J.H. Van Helden, F. Bénédic, Effect of the admixture of N<sub>2</sub> to low pressure, low temperature H<sub>2</sub>-CH<sub>4</sub>-CO<sub>2</sub> microwave plasmas used for large area deposition of nanocrystalline diamond films, *J. Phys. D. Appl. Phys.* (2020). doi:10.1088/1361-6463/aba7df.
- [21] A.P. Bolshakov, V.G. Ralchenko, G. Shu, B. Dai, V.Y. Yurov, E. V. Bushuev, A.A. Khomich, A.S. Altakhov, E.E. Ashkinazi, I.A. Antonova, A. V. Vlasov, V. V. Voronov, Y.Y. Sizov, S.K. Vartapetov, V.I. Konov, J. Zhu, Single crystal diamond growth by MPCVD at subatmospheric pressures, *Mater. Today Commun.* (2020). doi:10.1016/j.mtcomm.2020.101635.
- [22] A. Gicquel, M. Chenevier, K. Hassouni, A. Tserepi, M. Dubus, Validation of actinometry for estimating relative hydrogen atom densities and electron energy evolution in plasma assisted diamond deposition reactors, *J. Appl. Phys.* 83 (1998) 7504–7521. doi:10.1063/1.367514.
- [23] A. Dato, V. Radmilovic, Z. Lee, J. Phillips, M. Frenklach, Substrate-free gas-phase synthesis of graphene sheets, *Nano Lett.* 8 (2008) 2012–2016. doi:10.1021/nl8011566.
- [24] M. Tsuda, M. Nakajima, S. Oikawa, Epitaxial Growth Mechanism of Diamond Crystal in CH<sub>4</sub>-H<sub>2</sub> Plasma, *J. Am. Chem. Soc.* 108 (1986) 5780–5783. doi:10.1021/ja00279a019.
- [25] P.W. May, Y.A. Mankelevich, Experiment and modeling of the deposition of ultrananocrystalline diamond films using hot filament chemical vapor deposition and Ar/CH<sub>4</sub>/H<sub>2</sub> gas mixtures: A generalized mechanism for ultrananocrystalline diamond growth, *J. Appl. Phys.* (2006). doi:10.1063/1.2214304.
- [26] N. Paik, Raman and XPS studies of DLC films prepared by a magnetron sputter-type negative ion source, *Surf. Coatings Technol.* (2005). doi:10.1016/j.surfcoat.2004.08.073.
- [27] Y. Cai, R.Y. Wang, H.D. Liu, C. Luo, Q. Wan, Y. Liu, H. Chen, Y.M. Chen, Q.S. Mei, B. Yang, Investigation of (Ti:N)-DLC coatings prepared by ion source assisted cathodic arc ion-plating with varying Ti target currents, *Diam. Relat. Mater.* (2016). doi:10.1016/j.diamond.2016.09.003.
- [28] L. Vandenbulcke, T. Gries, J.N. Rouzaud, Nanodiamonds in dusty low-pressure plasmas, *Appl. Phys. Lett.* 94 (2009) 044106. doi:10.1063/1.3075604.
- [29] J. Biener, U.A. Schubert, A. Schenk, B. Winter, C. Lutterloh, J. Küppers, A surface reaction with atoms: Hydrogenation of sp- and sp<sup>2</sup>-hybridized carbon by thermal H(D) atoms, *J. Chem. Phys.* 99 (1993) 3125–3128. doi:10.1063/1.465166.